Through-Thickness Cleavage Fracture Stress of a Ti-V-N Plate Steel

Jun Sun and J.D. Boyd

Through-thickness cleavage fracture stresses, σ_f^*, have been determined for six microstructures of a Ti-V-N plate steel directly by through-thickness four-point bending (4PB) notched specimens. Results showed that σ_f^* is higher for ferrite-bainite microstructures than for ferrite-banded pearlite. For an identical finish-rolling temperature (FRT), the plates with a high cooling rate have a higher value of σ_f^* than their counterparts with a low cooling rate. Following the same cooling rate, the highest values of σ_f^* are obtained for steels finish rolled above A_{r3} but below T_{NR} (nonrecrystallization) and the lowest for steels finish rolled below A_{r3}, which contain deformed ferrite (DF) with texture components. Cleavage microcracks are observed to initiate at second-phase particle or pearlite-ferrite interface and then to propagate into ferrite matrix. Growing microcracks could be arrested by bainite phase distributed uniformly in ferrite matrix, which contributes to a high value of σ_f^*. The low value of σ_f^* was attributed to elongated ferrite-deformed ferrite and martensite/austenite (MA) microstructures.

Keywords cleavage fracture stress, microstructure, plate steel, through-thickness

1. Introduction

It is well established that thermomechanical processing (TMP) of steel, in particular, at low finish-rolling temperature (FRT), produces optimum combinations of high strength and toughness in the longitudinal direction related to the presence of various texture components formed parallel to the rolling plane. In the first case, appreciable saving in construction costs can be achieved by employing stronger materials and reducing the plate thickness. However, the textures significantly lowered the local cleavage fracture stress acting on this plane and also led to an increase in the density of rolling plane delaminations.[1] As a consequence, delamination has been observed in a variety of TMP microalloyed steel plate, and the lower the FRT, the greater the density of the delamination, for example, after an intercritical rolling. The occurrence of delamination has been correlated with reduction in both impact energy and through-thickness strength of rolled steel plate.[2–5] Therefore, with the increased interest in higher strength and toughness of the longitudinal direction, more attention is being paid to the consideration of through-thickness strength and toughness of rolled steel plate[5,6] because of lamellar tearing in heavy-section, welded structures, notable offshore drilling platforms.

The fracture mode of delaminations is mainly brittle cleavage[7,8] and follows a critical cleavage fracture stress criterion in the through-thickness direction.[9,10] The cleavage fracture stress is anisotropic for controlled rolled plate. Recently, quantitative research showed[1] that the anisotropy of cleavage fracture stresses increases with decreasing FRT and is related to their microstructures. However, in the through-thickness direction, the highest cleavage fracture stress is always achieved by plates finished-rolled below T_{NR} but just above A_{r3}, even though the highest value of σ_f^* is only 85% of the longitudinal one. By contrast, much less is known about the role of rolled microstructures on the delamination resistance of the plates. Furthermore, it is necessary to know if the through-thickness cleavage fracture stress of rolled plates could be improved considerably by suitable rolling schedules combined with some cooling method after rolling and how the cleavage fracture stress is affected by microstructures of rolled plates.

The aim of the project reported here is to investigate quantitatively the effect of different rolled microstructures on the through-thickness cleavage fracture stress of the steel plate and to try to evaluate the acceptability of the TMP parameter in the production of delamination-resistance steel plates for some specific application.

Jun Sun, State Key Laboratory for Mechanical Behavior of Materials, Department of Materials Science and Engineering, Xi'an Jiaotong University, Xi'an 710049, People's Republic of China; and **J.D. Boyd,** Department of Materials and Metallurgical Engineering, Queen's University, Kingston, ON, Canada K7L 3N6. Contact e-mail: junsun@xjtu.edu.cn.

2. Experimental

A microalloyed Ti-V-N steel plate with a thickness of 25 mm was used, which is a typical one for offshore application. The composition of the steel is given in Table 1. The experimental steel plate was produced by rolling slabs of this steel by three different rolling schedules (FRT = 950, 830, and 700 °C), *i.e.*, completely recrystallized rolling, nonrecrystallized rolling, and intercritical rolling, respectively, followed by either air cooling or water quenching. Six microstructures were produced by the TMP conditions above and are referred to as B1, B2, . . . , B6, respectively. A detailed description of the processing of the plate was given in Ref 11.

All specimens were single-edge-notched and tested in four-point bending (SEN-4PB) at −196 °C on an Instron universal testing machine with a crosshead speed of 0.5 mm/min. They were all of through-thickness orientation, *i.e.*, the fracture plane was parallel to the rolling plane, and crack propagation was in the longitudinal direction. Stubs were friction welded on the plate for the through-thickness tensile samples. The SEN-4PB specimen was an 8 mm square bar with a notch, located at the midthickness plane of the plates, of 3 mm depth, 45° flank angle, and notch radius $\rho = 0.25$ mm. The fracture surface of each fractured sample was examined by scanning electron microscopy (SEM). A few double-notched 4PB samples (DNB) were used to observe the nonpropagating microcracks ahead of the uncracked notch. The complete description of the finite element method calculation and the determination of σ_f^* have been presented in a previous study.[1]

3. Results

3.1 Microstructures of Rolled Plate

The microstructures of the rolled plate are shown in Fig. 1. Recrystallization rolling (FRT = 950 °C) produced ferrite (F)-pearlite (P) in the air-cooled (AC) plate (Fig. 1a) and ferrite-bainite (B) in the water-quenched (WQ) plate (Fig. 1b). The ferrite grain size is smaller in the WQ plate than in the AC plate. There are identical microstructural components but smaller ferrite grains in plates finish rolled below T_{NR} but above A_{r3} (Fig. 1c and d). Pronounced banding pearlite was presented in the AC plates (Fig. 1a and c) and a little martensite/austenite (MA) in the WQ plates (Fig. 1b and d). For finish rolling in the intercritical region, AC plate contained heavily banded pearlite, ferrite, and deformed ferrite (DF) (Fig. 1e) and WQ plate had ferrite, DF, and martensite (Fig. 1f).[11] The results of the quantitative metallography measurements for six plates are reported in Table II. The average ferrite grain diameter, D_A, and the ferrite grain diameter vertical to the through-thickness of the plates, D_{TT}, were determined by an image analyzer.

3.2 Through-Thickness Cleavage Fracture Stress

The measurements of the through-thickness cleavage fracture stress σ_f^* for the six plates are given in Fig. 2. Generally, σ_f^* of WQ plate is higher than that of its AC counterpart individually because of refinement of ferrite grains in WQ plate and the presence of banded pearlites in AC plate. For each cooling treatment, either AC or WQ, σ_f^* is lowest for plates rolled below A_{r3}, which contain heavily banding structures, and is highest for plates nonrecrystallization rolled, containing about 30% bainite (+martensite) distributed uniformly in the matrix of about 70% refined ferrite. The optimum value of σ_f^* was presented by plates finish rolled about the midsection between T_{NR} and A_{r3} and WQ.

3.3 Fractography

Figure 3 presents some cleavage initiation sites on the fracture surface of specimens. Generally, at the origin of cleavage facet, a second-phase particle can be found, which means the cleavage microcracks were initiated there. Cleavage facets are more flat and larger in diameter for plates rolled below A_{r3} (Fig. 3c and d) than for plates rolled above A_{r3} (Fig. 3a and b), which were associated with either lower or higher σ_f^* individually.

3.4 Nonpropagating Microcrack

The nonpropagating cleavage microcracks were observed at a distance of some hundred microns from the root of uncracked notches of DNB specimens for six plates. For B1 plate with ferrite-banded pearlite microstructure, it can be seen that a microcrack initiated at the interface of ferrite and pearlite and then propagated into neighboring ferrite grains, as shown in Fig. 4(a). The nonpropagating microcrack has a length of about 40 μm and spans about two ferrite grains. The propagation of the microcrack was on the plane parallel to the rolling plane and perpendicular to the maximum tensile principal stress direction. For B2 plate with a microstructure of ferrite and bainite, as given in Fig. 4(b), a microcrack initiated from a second-phase particle on the interface, grew through a ferrite grain, reached the interface to a bainite grain, and was arrested there. Figure 4(c) shows that, in plate B4, a microcrack propagated through some ferrite grains and small bainitic regions and stopped on both a ferrite grain boundary and another bainitic region.

4. Discussion

The process of the cleavage fracture is described as follows: when the applied load is increased, slips occur in the grain in the vicinity of the notch root or precrack tip, and dislocations move and pile up at the boundaries of the second-phase (particles) or inclusions, which act as a barrier to slip bands.[12,13] Then, the microcrack is initiated and extends stable through the matrix. With the increase in the length of the microcrack, the normal stress σ_{yy} ahead of it increases due to the increase

Table 1 Chemical composition of experimental steel (weight percent)

C	Mn	Si	S	P	Al	Ti	V	N	O
0.08	1.26	0.29	0.005	0.003	0.04	0.01	0.08	0.012	0.009

Table 2 Quantitative metallography (%) and room-temperature yield strength of plates

Plate	FRT/Cooling	F	DF	P	B + MA	D_A (μm)	D_{TT} (μm)	σ_y (MPa)
B1	950/AC	87.9	…	12.1	…	31.4	32.6	283.0
B2	950/WQ	69.8	…	3.0	27.2	20.7	21.8	443.0
B3	830/AC	90.2	…	9.0	0.8	15.2	15.6	334.0
B4	830/WQ	66.1	…	6.8	27.1	14.8	15.8	382.0
B5	700/AC	34.5	54.6	9.8	1.1	11.3	34.2	448.0
B6	700/WQ	24.3	62.2	…	13.5	10.7	35.2	505.0

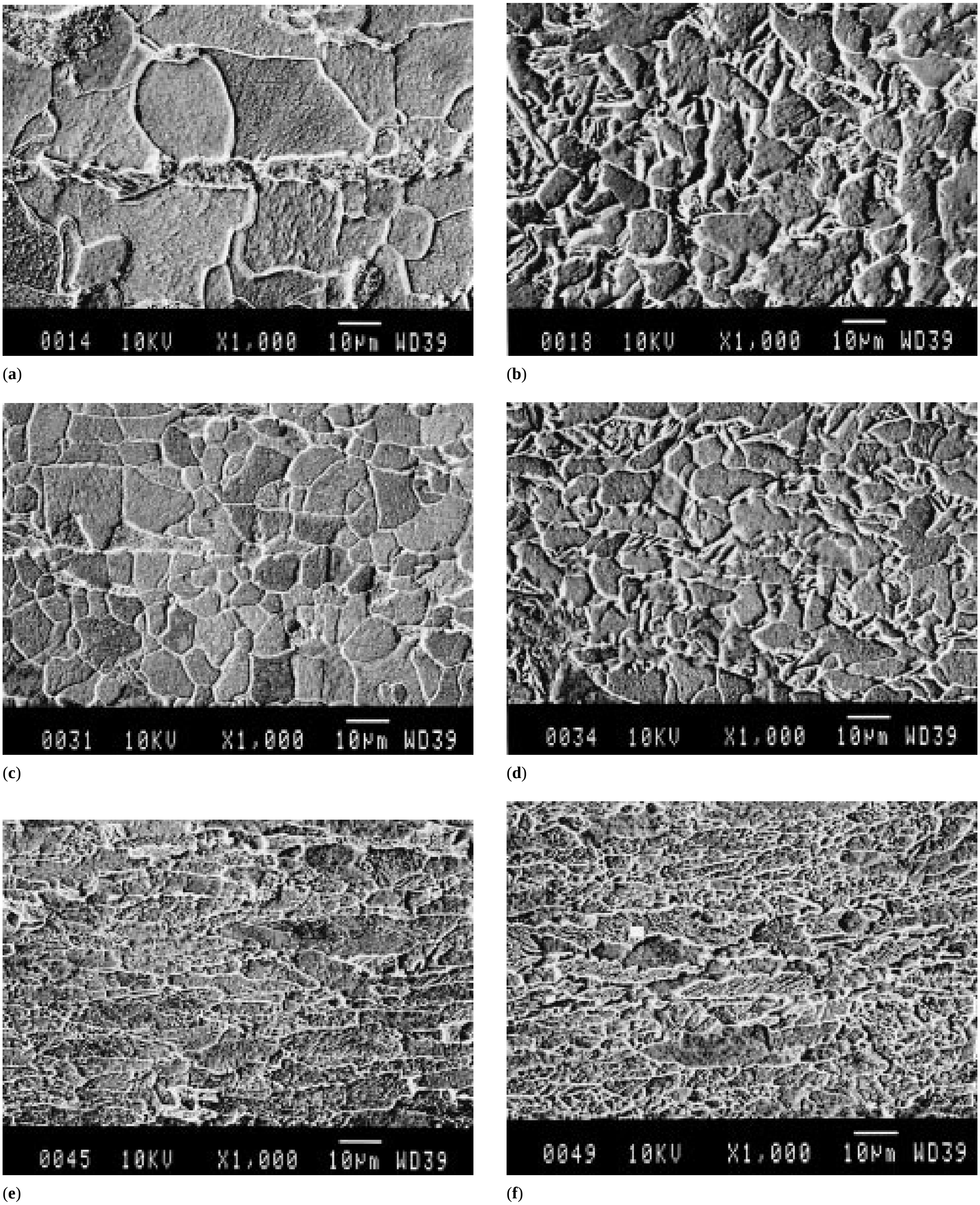

Fig. 1 Microstructures of the rolled plates: (**a**) FRT = 950 °C, air cooling; (**b**) FRT = 950 °C, water quenching; (**c**) FRT = 830 °C, air cooling; (**d**) FRT = 830 °C, water quenching; (**e**) FRT = 700 °C, air cooling; and (**f**) FRT = 700 °C, water quenching

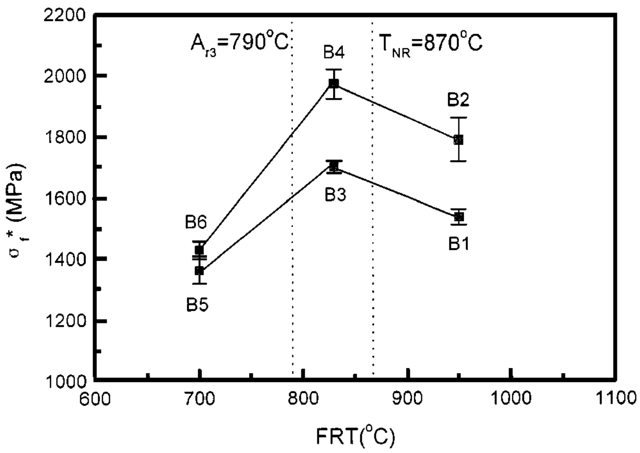

Fig. 2 Variation in σ_f^* with FRT and cooling method

of applied load. When the $\sigma_{yy} > \sigma_f^*$ (local cleavage fracture stress), the cleavage fracture occurs. At a low temperature, the dislocation-induced microcrack could extend catastrophically without the stage of stable propagation.[14] The critical event of cleavage in steel is considered to be the unstable extension of the microcrack with critical length.[15] And the critical event is either the propagation of ferrite grain-sized microcrack[14,15] or that of a second-phase particle-sized microcrack.[12,13] Consequently, the values of σ_f^* will be dominated by the critical lengths of the microcracks, which depend directly on the microstructures of steels tested.

The present study shows that the microcracks were initiated at the second-phase particle or interface among two phases and propagated into one or two ferrite grains and mostly arrested on grain boundaries (Fig. 4c) or the interface of hard phases (Fig. 4b). Some of them were arrested midway in an entire ferrite grain (Fig. 4a). Recent work[14] indicated that there was no clear correlation of σ_f^* to sizes of particles initiating cleavage

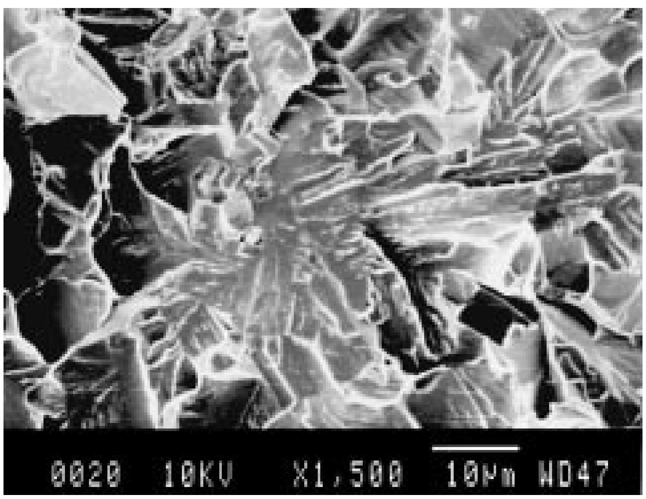

(**a**)

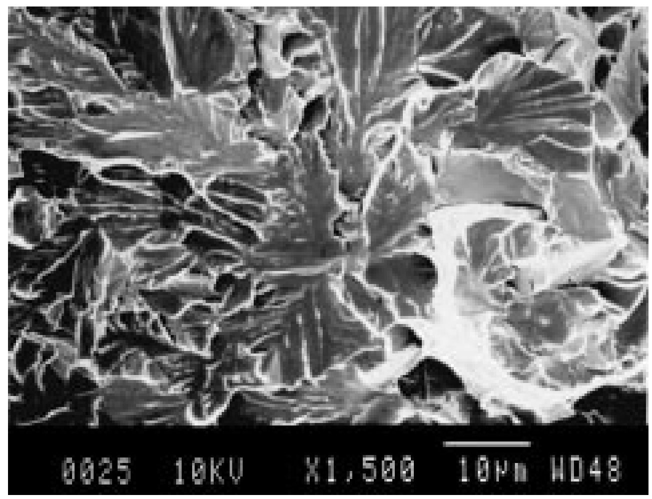

(**b**)

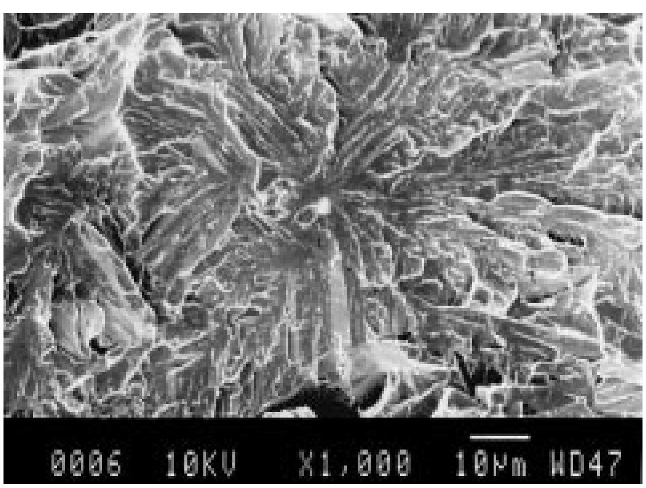

(**c**)

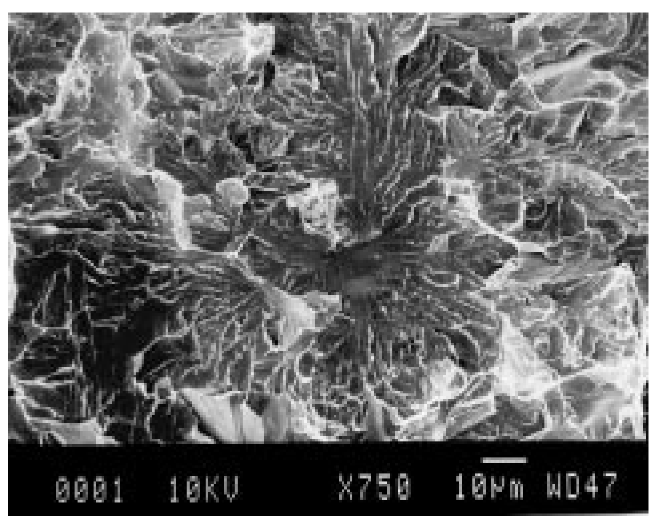

(**d**)

Fig. 3 Fracture surface of specimens showing cleavage initiation sites: (**a**) B3, (**b**) B4, (**c**) B5, and (**d**) B6

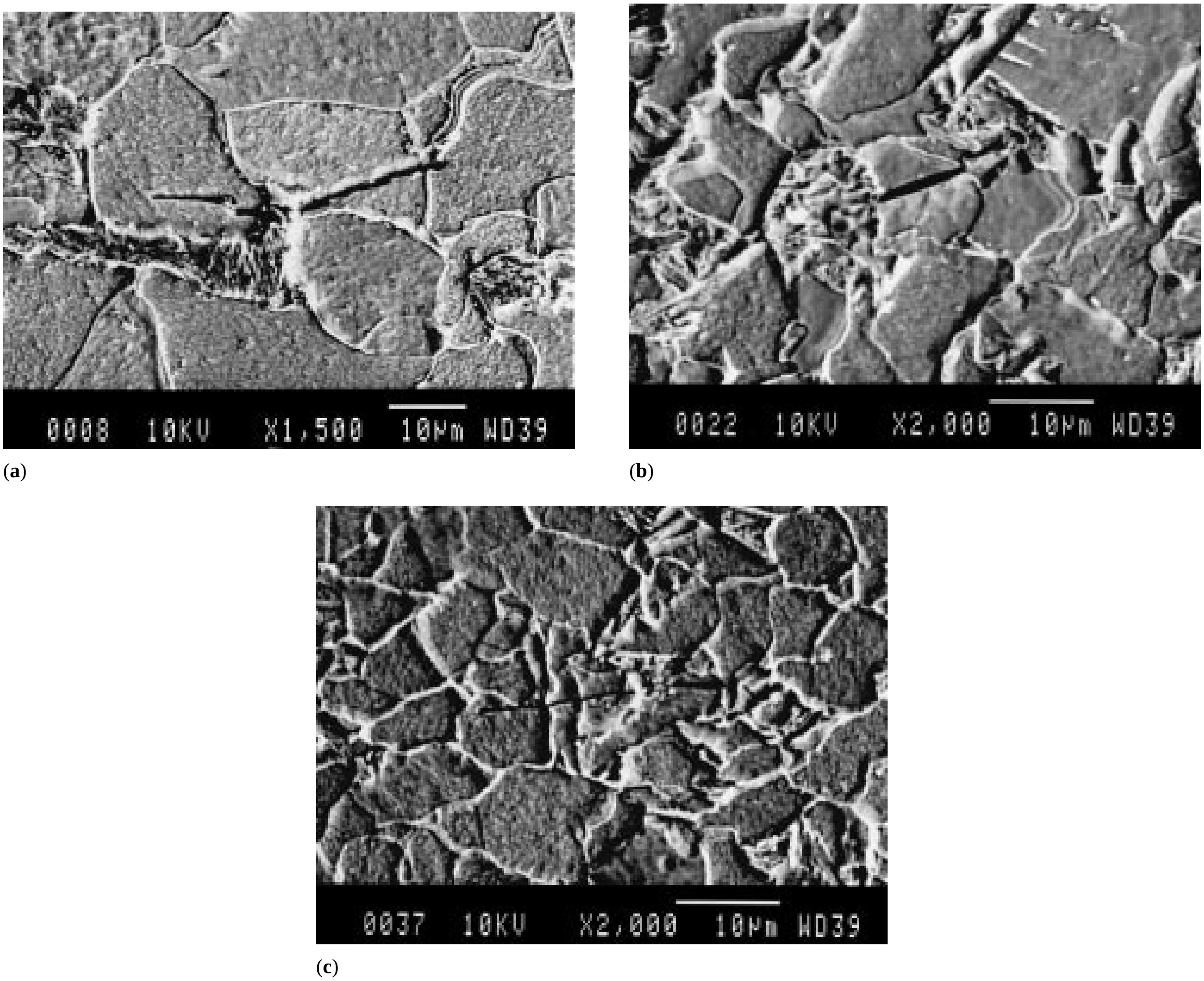

Fig. 4 SEM metallographic sections showing nonpropagating microcracks in double-notch 4PB specimens: (**a**) B1, (**b**) B2, and (**c**) B4. Maximum principal tensile stress is vertical

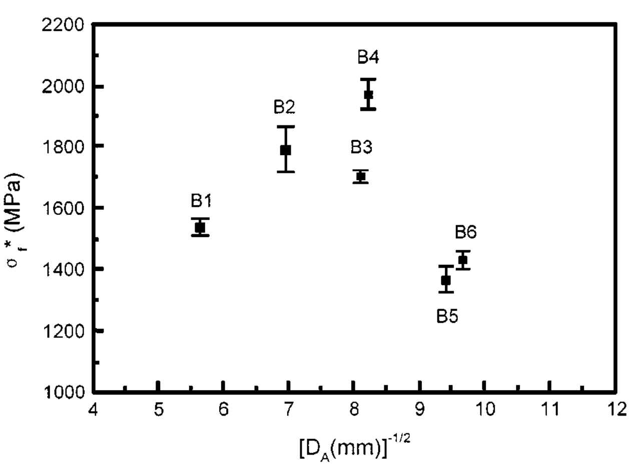

Fig. 5 Relation between average σ_f^* and mean ferrite grain diameter D_A

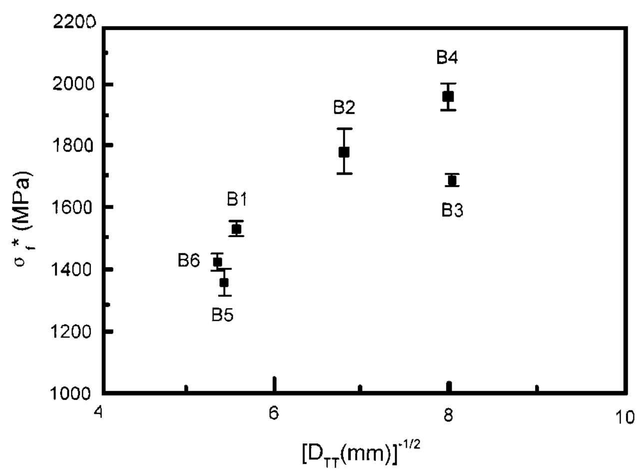

Fig. 6 Relation between average σ_f^* and mean ferrite grain diameter on rolling plane D_{TT}

and the critical event was the propagation of a ferrite grain-sized crack into the neighboring matrix. The σ_f^* is mainly determined by the size of ferrite grain. Because the fine grain has a smaller ferrite grain compared with the coarse grain, the fine grain has a higher value of σ_f^*.[14,16,17] However, the conclusion is only drawn from the steels with normalized microstructure and is not generally applicable to the steels with hot-rolling microstructures investigated presently.

Plotting the measured σ_f^* for the 4PB test against the average diameter of ferrite grains of six steels in Fig. 5, it is revealed that σ_f^* is not regularly related to the average diameter of ferrite grains, although there is an upward, almost linear tendency in σ_f^* of B1, B2, and B4 plates with the decrease in sizes of ferrite grains. For example, the value of σ_f^* in B4 steel is much higher than that in B3 steel, even though both steels have similar average ferrite grain diameters. Furthermore, the average diameter of ferrite grains in B2 steel is greater than that in B3 steel, but B2 steel has a higher value of σ_f^* than does B3 steel. Particularly, for B5 and B6 steels, having the smallest average diameter of ferrite grains, the values of σ_f^* are the lowest values. The linear relation, however, between σ_f^* and ferrite grain sizes can be obviously improved when the anisotropic dimension of ferrite grains, D_{TT}, is taken into account, as shown in Fig. 6.

Actually, for multiphase microstructures, the process of cleavage fracture at low temperature is complex and is unlikely to be determined by only one factor, *i.e.*, ferrite grain size. In dual-phase alloys, the plastic incompatibility between soft and hard phases causes high local stress and strain concentrations, which may lead to premature fracture by void or microcrack initiation and propagation.[19–21] For ductile damage of materials, experiments suggest that the constraint induced by the hard phase on the adjoining matrix and the consequent development of matrix triaxiality not only influence the apparent flow strength of the materials, but also promote ductile void growth.[17,18] For brittle cleavage fracture, a similar situation exists, as shown in Fig. 4(a). The microcrack initiated at the upper interface between pearlite and ferrite, grows into the adjacent ferrite matrix, which could be elucidated by the finite element simulations of dual-phase microstructure models.[22–24] It can be seen that within the hard phases the hydrostatic tensile stress, σ_m/σ_o, or constraint and effective tensile stress are relatively uniform and low, whereas the high level of σ_m/σ_o has been generated in the matrix by the constraint of hard phases. The highest level of σ_m/σ_o occurs in the matrix near the interface with the sharp top (bottom) corner of the hard phase along the line of loading through the corner. The present result supports the proposition that the hydrostatic tensile stress plays an important role in the damage initiation in multiphase materials.

On the other hand, the propagation of microcracks in cleavage should also be influenced by the distribution of σ_m/σ_o. On the cracking path, for example, of B2 and B4 steels, a hard phase with low level of σ_m/σ_o will reduce the effective stress intensity factor, K_{eff}, ahead of the microcrack and arrest the microcrack on the way at the interface. Much higher applied stress will be required to increase the level of K_{eff} of the microcrack until the final cleavage fracture occurs, whereas a higher value of σ_f^* has been obtained by the steels. However, for the banded structures, slight or heavy, the microcracks grow into adjacent matrix after they initiate at the phase interface as the applied stress level is increased. When the critical length, associated with some maximum principal tensile stress, is reached by the microcrack, the cleavage fracture occurs because there is no hard phase existing along the way to stop the crack. For B1 and B3 steels, intermediate values of σ_f^* have been obtained because the majority of microstructure constituents are ferrite, which can deform plastically to release the high σ_m/σ_o. The B5 and B6 steels have the lowest values of σ_f^* because not only the hard phase has a volume fraction of 60 to 70%, as a brittle-matrix composite, which constrained the capability of ferrite deformation, but also the heavily banded structures provide a continuous path for cleavage microcracks by numerous interfaces with high σ_m/σ_o in the adjacent matrix.

In summary, the refinement of ferrite grains contributes to the increase in σ_f^*, *i.e.*, σ_f^* (B3) $>$ σ_f^* (B1) and σ_f^* (B4) $>$ σ_f^* (B2) $>$ σ_f^* (B1). However, much more enhancement in σ_f^* is attributed to the presence of hard phases, for instance, bainites distributed uniformly in microstructures, *i.e.*, σ_f^* (B2) $>$ σ_f^* (B3), even though B2 steel has a greater grain size than that of B3 steels, and σ_f^* (B4) $>$ σ_f^* (B3), although B4 steel has similar grain size to that of B3 steel. The heavily banded structures are detrimental for the through-thickness cleavage fracture stress of rolled plates.

6. Conclusions

- The highest values of σ_f^* are found for steels having FRT between T_{NR} and A_{r3}, and the lowest values of σ_f^* are obtained when FRT is below A_{r3}. Steels having FRT above T_{NR} exhibit intermediate values of σ_f^*.
- The values of σ_f^* for WQ plate are constantly higher than for the corresponding AC plate because of smaller ferrite grain size, in particular, the bainite resulted from the water-quenching process.
- The highest value of σ_f^* is obtained for a dual-phase microstructure of bainite (+martensite) distributed uniformly in fine-grained ferrite, *i.e.*, B4 steel.
- In the heavily banded microstructures (B5 and B6), the continuous path for the cleavage fracture in the PF results in the lowest value of σ_f^*.

Acknowledgments

Financial support from NSF of China and NSERC Canada is gratefully acknowledged. This work was also supported by the NSERC International Research Fellowship of Canada and the National Outstanding Young Investigator Grant of China.

References

1. J. Sun and J. Boyd: *Proc. 36th Mechanical Working and Steel Processing Conf.,* ISS-ASME, Warrendale, PA, 1995, vol. XXXII, pp. 495-501.
2. B. Faucher and B. Dogan: *Metall. Trans. A,* 1988, vol. 19A, pp. 505-16.
3. G.J. Baczynski, J.J. Jonas, and L.E. Collins: *Metall. Mater. Trans. A,* 1999, vol. 30A, pp. 3045-54.
4. H. Hero, J. Evensen, and J.D. Embury: *Can. Metall. Q.,* 1975, vol. 14, pp. 117-22.

5. D.M. Fegredo: *Can. Metall. Q.*, 1975, vol. 14, pp. 243-55.
6. B. Dogan and J.D. Boyd: *Metall. Trans. A*, 1990, vol. 21A, pp. 1177-91.
7. B. Engl and A. Fuchs: *Proc. 4th Eur. Conf. on Fracture*, Chameleon Press, London, 1982, pp. 335-42.
8. P. Brozzo, G. Buzzichelli, A. Mascanzoni, and M. Mirable: *Met. Sci.*, 1977, vol. 11, pp. 123-29.
9. K. Kuhne, H. Dunnewald, and W. Dahl: *4th Eur. Conf. on Fracture,* Chameleon Press, London, 1982, pp. 329-34.
10. G. Baldi and G. Buzzicheli: *Met. Sci.*, 1978, vol. 12, pp. 459-72.
11. B. Dogan, L.E. Collins, and J.D. Boyd: *Metall. Trans. A,* 1988, vol. 19A, pp. 1221-34.
12. A.H. Cottrell: *Trans. AIME,* 1958, vol. 212, pp. 192-98.
13. C.J. McMahon and M. Cohen: *Acta Metall.*, 1965, vol. 13, pp. 591-604.
14. J.H. Chen, L. Zhu, and Z. Wang: *Metall. Trans. A,* 1993, vol. 24A, pp. 659-67.
15. D.A. Curry: *Met. Sci.,* 1980, vol. 14, pp. 319-26.
16. Tsann Lin, A.G. Evans, and R.O. Ritchie: *Metall. Trans. A,* 1987, vol. 18A, pp. 641-51.
17. C. Yan, C.H. Chen, J. Sun, and Z. Wang: *Metall. Trans. A*, 1993, vol. 24A, pp. 1381-89.
18. J. Sun, Z.J. Deng, and M.J. Tu: *Chinese J. Mech. Eng.*, 1991, vol. 4, pp. 258-64 (in English).
19. X.L. Cai, J. Feng, and W.S. Owen: *Metall. Trans. A,* 1985, vol. 16A, pp. 1405-15.
20. W.C. Jeong and C.H. Kim: *Metall. Trans. A,* 1988, vol. 19A, pp. 309-17.
21. D.L. Steinbrunner, D.K. Matlock, and G. Krauss: *Metall. Trans. A,* 1988, vol. 19A, pp. 579-89.
22. Z.H. Li and H.C. Gu: *Metall. Trans. A,* 1991, vol. 22A, pp. 2695-2702.
23. T. Christman, A. Needleman, and S. Suresh: *Acta Metall.,* 1989, vol. 37, pp. 3029-50.
24. X.Q. Xu and D.F. Watt: *Acta Metall.,* 1994, vol. 42, pp. 3717-29.